Frontogenesis and Symmetric Stability in a Major New England Snowstorm

FREDERICK SANDERS*

9 Flint Street, Marblehead, MA 01945

(Manuscript received 27 January 1986, in final form 31 March 1986)

ABSTRACT

Synoptic and Doppler radar data are used to study the roles of large-scale frontogenetical forcing and of moist symmetric instability in the New England snowstorm of 5–6 December 1981, associated with an explosively intensifying cyclone offshore. Radar reflectivity patterns showed a tendency toward banded structure, particularly near the leading (northwestern) edge of the storm. Only a minor portion of the snowfall, however, was associated with this pronounced bandedness.

From a set of constant-pressure analyses, the frontogenetical forcing was measured from the variation along the temperature gradient of the geostrophic wind component in the direction of this gradient. Over southeastern New England maximum forcing, found near 500 mb at the outset of the storm, descended to the layer between 850 and 700 mb 24 h later. Magnitudes were (3–7) $\times 10^{-10}$ deg m^{-1} s^{-1}. Observed rates of strengthening of temperature gradient were less than half this value, implying relative adiabatic cooling in the rising warmer air. Doppler radar observations showed strong convergence just above the zone of maximum frontogenesis and at the base of a region of vigorous ascent, with magnitude of a few tens of cm s^{-1}.

Symmetric stability was evaluated, for a geostrophic base-state flow, from a series of vertical cross sections as close as possible to the radar site. Only small areas of instability appeared in the saturated middle and upper troposphere near the outset of the storm. An evaluation based on gradient-wind balance, on the assumption that the base-state flow locally represented a portion of a steady circular vortex, enlarged these regions of small or negative stability in the northwestern portions of the major cloud mass. Strong (moist or dry) symmetric stability was indicated, however, in the inner portions of the developing cyclonic circulation.

The small stability initially accompanying the frontogenetical forcing was consistent with recent analytic and numerical models showing a vigorous and concentrated frontal updraft. Details of the structure shown by the Doppler data, and in particular the prominence of the bandedness at the northwestern edge of the storm, could be attributed to symmetric instability. The ascent was driven, however, by the frontogenetical forcing, but with an intensity and sharpness due to the small stability of the warmer air.

1. Introduction

Organization of the widespread precipitation of cyclonic storms into mesoscale lines has received increasing attention in the past few years. The traditional view (e.g., Bjerknes, 1919) was that, whereas rain associated with a cold front was organized into a narrow line of showers, the warm front produced a broad shield of relatively gentle precipitation. The ubiquity of bandedness in cyclonic precipitation, evident in early studies by Sawyer (1952), Elliott and Hovind (1964), Kreitzberg (1968) and Browning and Harrold (1969), for example, has been underscored by Herzegh and Hobbs (1980) even for the warm frontal region.

Among theoretical explanations of these bands, moist symmetric instability in saturated air has been elucidated recently by Bennetts and Hoskins (1979) and by Emanuel (1983a,b). On the other hand, small but positive moist symmetric stability was shown by Emanuel (1985) to be conducive to increasing the intensity and reducing the scale of the updraft driven by large-scale frontogenetical forcing. Numerical calculations of this situation by Thorpe and Emanuel (1985) show that latent heating can readily be concentrated on a mesoscale for a modest value of moist symmetric stability.

The relative roles of these two mechanisms may be difficult to sort out observationally, as indicated by Thorpe and Emanuel (1985). The difficulty seems to arise most obviously when the observations are limited to radar echoes, satellite images and raingage catches. In principal the synoptic-scale soundings can be used to assess the symmetric stability and to measure the frontogenetical forcing. Sanders and Bosart (1985a) undertook to do this for a major snowstorm in the northeastern United States, finding that the major precipitation band was a consequence of the forcing, but that symmetric instability was likely responsible for transient structure of the upper portions of the cloud mass and for the final fragmentation of the major band.

Multiple bandedness at first glance does not suggest frontogenetical forcing alone. Hoskins et al. (1984) investigated numerically whether a large-scale fronto-

* Former affiliation: Department of Meteorology and Physical Oceanography, Massachusetts Institute of Technology.

genetical wind field, acting on an initial temperature field containing parallel regions of maximum horizontal gradient, would produce multiple frontal bands. They found that individual frontal updrafts were distinct only at low levels and merged into a single cloud mass above. Numerical modeling by Hsie et al. (1984) suggests that the production of multiple rainbands may have been attributable to symmetric instability. Hence the first glance seems correct.

In an attempt to assess the possibility of band formation as a consequence of symmetric instability alone, without involvement of a frontal mechanism, Seltzer et al. (1985) selected a number of winter storm cases, observed by the Massachusetts Institute of Technology (MIT) radar, in which neither surface fronts nor the surface low-pressure center was nearby. The 11 banded cases were found to contain layers of symmetric instability 0.5 to 2.0 km deep. The bands were oriented nearly along the thermal wind. Only four cases were found to display multiple bands, however, and frontogenetical aspects were not examined at upper levels.

Here we wish to look in depth at one of the cases in the group examined by Seltzer et al. (1985). This case was also studied by Passarelli et al. (1986), who concurred with the finding of symmetric instability as the source of the band. Again the absence of "obvious surface fronts over the New England region" was evidently taken as indicating the unimportance of a frontal mechanism. It is this mechanism we wish to evaluate directly, looking also at symmetric instability in a somewhat different way.

2. The storm of 5–6 December 1981

Explosive cyclogenesis occurred on 5–6 December some 500 km off the East Coast of the United States. The deepening cyclone center, as seen in the NMC analyses in Fig. 1, moved north-northeastward to a position about 400 km east of the MIT radar by 1200 GMT on the 6th, casting a blanket of heavy snow over most of New England. By visually inspecting the density of intersection points between sea level isobars and thickness lines, one can see a region of maximum warm advection, growing in strength as the storm intensified, and moving slightly west of northward, its centroid passing east of New England. To the west, there was little advection. Since the thickness lines were oriented more or less meridionally, it is clear that in a broad sense horizontal advection was acting to strengthen the temperature gradient across New England during the storm. That is, there was frontogenetical forcing.

It is clear from the maps in Fig. 1 that there was substantial variation along the thickness lines in the geostrophic component normal to them. The two dimensionality usually assumed in frontogenetical theory is not justified. Nevertheless, the cross-isotherm variation of geostrophic wind, which we shall use as a measure of frontogenetical forcing, is contained within the

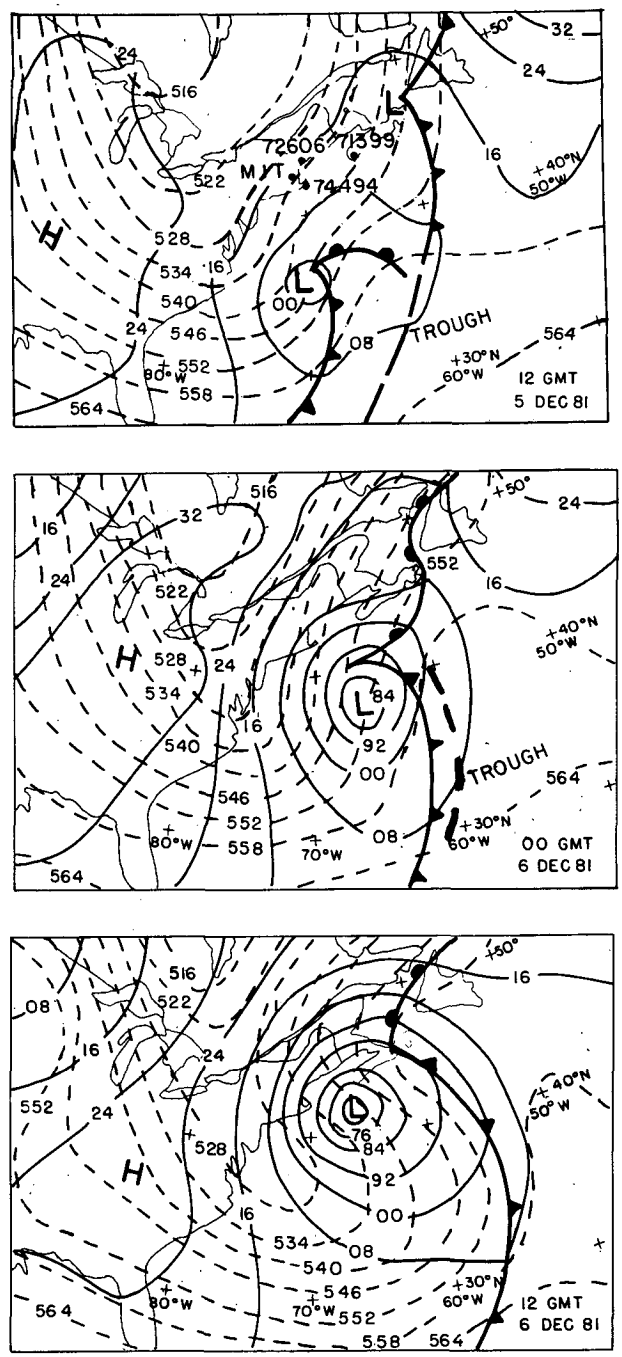

FIG. 1. Isobars of sea level pressure (solid) at intervals of 8 mb and contours of thickness of the layer 1000–500 mb (dashed) at intervals of 6 dam with positions of surface fronts and centers of high and low pressure, adapted from analyses of the National Meteorological Center. (a) 1200 GMT 5 December 1981, (b) 0000 GMT 6 December 1981 and (c) 1200 GMT 6 December 1981.

Q-vector formulation (Hoskins and Pedder, 1980) of the general forcing function for the quasi-geostrophic omega equation, and its relevance is not limited to slab-symmetric situations. The remaining part of the

Q-vector, represented by the along-isotherm variation of the normal geostrophic component, would simply enhance the ascent where the warm advection is strongest. The effect of this variation would be also to rotate the isotherms in the counterclockwise sense, as observed.

Despite the paucity of thickness data over the ocean, the finding of frontogenesis seems inescapable, since as pointed out by Sutcliffe and Forsdyke (1950) the thickness analysis is subject to the constraints of climatological reasonableness and thermodynamical process. Moreover, that portion of the analysis that most affects New England reflects the available soundings at stations 71399 and 71600. The sounding from 74494 was missing at 0000 GMT on the 6th, but the upper-level analyses could not have been greatly different, since surface observations from ships and buoys were sufficiently numerous to provide an accurate analysis of sea level pressure, and the temperature sounding was observed 12 h earlier and later.

Snow depths produced by the storm are shown in Fig. 2, adapted from U.S. Dept. of Commerce (1981). Little precipitation fell in extreme southwestern Connecticut, and depths near the coast in Maine were limited because a portion of the precipitation fell as rain.

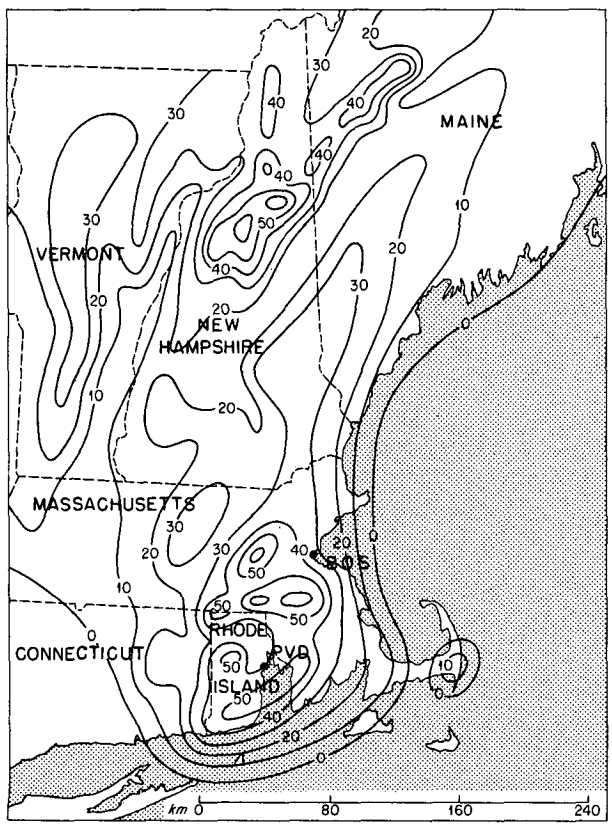

FIG. 2. Depth (cm) of total snowfall in the storm of 5–6 December 1981. (After U.S. Dept. of Commerce 1981.)

Many features of the pattern (e.g., the maxima between BOS and PVD, in the hills of southern New Hampshire and in the mountains of Vermont and western Massachusetts) resemble those found by Passarelli and Boehme (1983) to be typical of easterly rainstorms in New England and to be due to orographic influences. The strength of the maxima in eastern Massachusetts and particularly their extension in Rhode Island are anomalies to be addressed later.

A series of constant-altitude plan-position-indicator (CAPPI) maps for the layer from 2.5 to 4.0 km elevation, made from data obtained from the MIT radar, are presented in Fig. 3. A prominent band is seen approaching southeastern New England at 1157 GMT, at the leading edge of the storm. Sometimes distinct, other times diffuse, sometimes single, other times double, it could be tracked for at least 24 h. Isochrones of its center at 3-h intervals appear in Fig. 4. The orientation rotated counterclockwise during the period, as noted by Passarelli et al. (1986). In the present analysis this rotation was through nearly 90 deg in the period of study. Observe from Fig. 1 that the thickness lines over New England rotated similarly, so as to keep the band orientation parallel to the thermal wind. The position around 0000 GMT on the 6th was studied in detail by Seltzer et al. (1985) and by Passarelli et al. (1986). After this time the southern portion of the line, extending out to sea from southeastern New England, appeared detached from the northern portion and indeed appeared to have arisen from a different cause, as we shall see. Much of the CAPPI imagery, in contrast to the case reported by Sanders and Bosart (1985b), displayed a chaotic appearance. Tendencies toward bandedness, more or less pronounced, appeared from time to time, but without the spatial or temporal continuity displayed by the initial band.

The relationship of snowfall to the major band was not clear in the hourly surface observations. The start of the precipitation was nearly coincident with its arrival in southeastern Massachusetts, but later preceded it by 3–4 h as the 15-dBZ reflectivity contour moved northwestward more rapidly than the centroid of the band. An area of moderate or heavy rain or snow accompanied the arrival of the band at most stations in eastern Massachusetts and as far west as the Connecticut River Valley. (Several key stations between these areas did not make observations during the night.) Much later outbursts, 4–24 h after band passage, however, appeared to produce the bulk of the snow. The detailed record for Boston (BOS) (after U.S. Dept. of Commerce, 1981) seen in Fig. 5 shows little effect of the band passage around 0000 GMT 6 December, with a much more prominent precipitation episode 4–6 h later and three others after that. The associated radar echoes were clearly not part of the initial band. In New Hampshire the band produced a brief period of light snow but the heaviest amounts fell much later, as could be surmised from the CAPPI maps in Fig. 3. Overall,

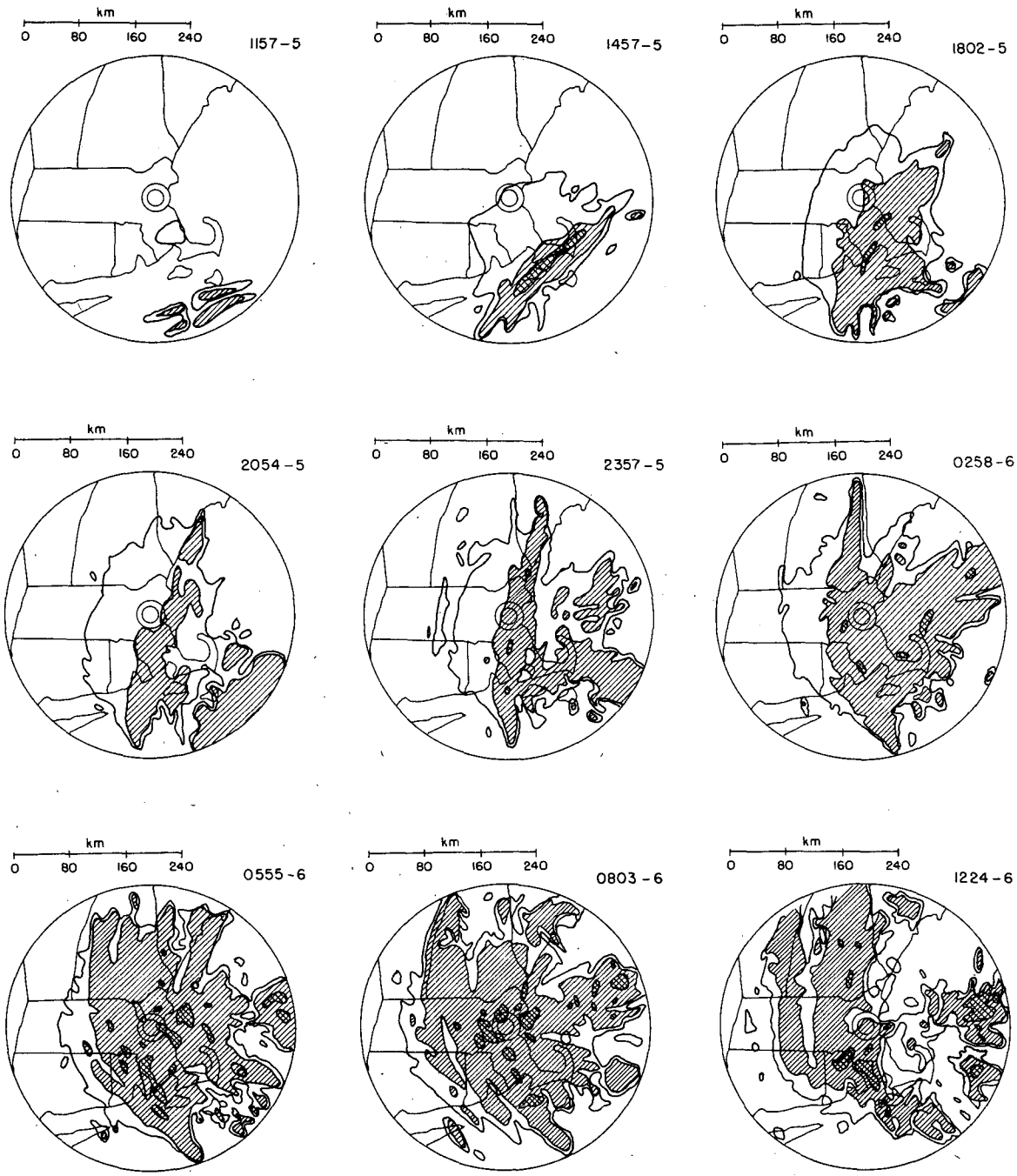

FIG. 3. CAPPI presentations for the layer 2.5–4.0 km from the MIT radar, December 1981. Reflectivity contours for 15, 25 and 35 dBZ are shown; single-hatching and cross-hatching delineate areas with values greater than 25 and 35 dBZ, respectively. GMT and date are indicated: 1157–5 denotes 1157 GMT on the 5th, and so forth.

the band was a minor contributor to the total precipitation.

3. Frontogenetical forcing

To provide a basis for calculations of the large-scale frontogenetical forcing over New England, a series of maps was analyzed: for the surface at 6-h intervals from 1800 GMT 4 December through 1200 GMT of the 6th, and for 850, 700, 500, 400 and 300 mb at 12-h intervals from 1200 GMT on the 5th through 1200 GMT on the 6th. Examples appear in Fig. 6.

The 500-mb analysis at the earliest time (Fig. 6a) shows anticyclonically curved southwesterly flow over

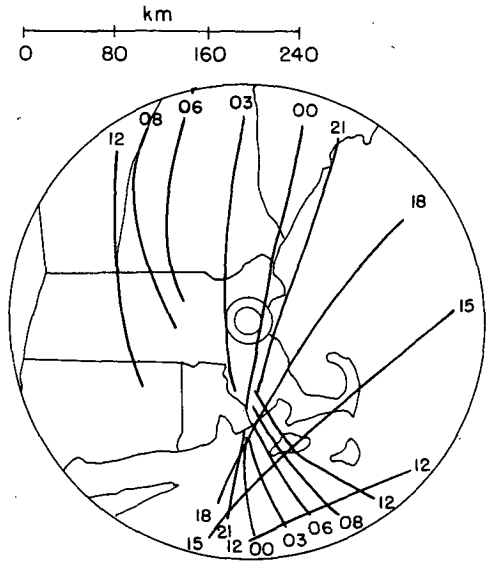

FIG. 4. Isochrones of time (GMT hours) of the position of the major radar band, from 1200 GMT 5 December to 1200 GMT 6 December, derived from the CAPPI presentations in Fig. 4.

southern New England, with speeds increasing from northwest to southeast. There was weak confluence as well. The estimated orientation of the dilatation axis in the deformation field would thus be rotated not quite 45 deg clockwise from the flow direction, nearly parallel to the isotherms. The pattern was evidently frontogenetical.

Twelve hours later (Fig. 6b), the approaching cyclone was apparent in the flow at 700 mb. There was little lateral shear, so far as we can estimate, but there was distinct diffluence in the east-northeasterly flow over the region of interest. The approximately meridional orientation of both dilatation axis and isotherms again indicated frontogenesis. At the last time (Fig. 6c), the explosive cyclogenesis offshore was accompanied by strong flow at 850 mb. The intensity of the pattern makes estimation of the deformation pattern difficult, but the northerly flow over southern New England appears to be characterized by confluence, again suggesting frontogenetical forcing.

Quantitative calculation of this forcing was carried out at all analyzed levels and times, at the nine interior points of a 5×5 grid. This grid was centered on MIT, with a nominal mesh length of 110.8 km. The orientation of the grid was adjusted on each map so as to make the rows normal to the isotherms. That is, the nominal x-axis was taken along the direction of the temperature gradient, as illustrated in Fig. 6. The frontogenetical forcing was then computed at each interior point by simple centered finite differences, from the expression $-(\delta u_g/\delta x)(\delta T/\delta x)$, where the subscript g refers to the geostrophic wind and δx is 221.6 km. The results, averaged over the nine interior points so as to produce values representative of the area viewed by the MIT radar and not strongly affected by small quirks of the subjective analysis and interpolation processes, are presented in Fig. 7, along with the direction and magnitude of ∇T (similarly averaged).

As anticipated from the general picture presented in Fig. 1, the forcing in Fig. 7a is almost everywhere frontogenetical. A well-defined maximum was observed near 500 mb at 1200 GMT on the 5th, strengthening and lowering to a level between 700 and 850 mb 24 h later. Values at the surface behaved somewhat independently, in part because the isotherms tended to follow the coastline, with warmer air offshore. The temperature gradient over the area, in Fig. 7b, strengthened during the period, with a descending maximum roughly following the maximum frontogenesis but not so well defined. The increase of magnitude was modest, however, in contrast to the rate given by the large-scale advection (Fig. 7a). The discrepancy implies that the warmer air was cooling adiabatically, owing to ascent, relative to the colder air. Additionally, the counterclockwise turning of the isotherms with time is apparent.

These calculations say nothing about the horizontal distribution of the forcing. Inspection of the advection patterns implied by the contours and isotherms in Fig. 6, however, suggests that the maxima in the vertical were also maxima in the horizontal. Thus, Fig. 7 can perhaps be regarded as a spatial section, in which the frontogenetical forcing qualitatively resembles that in Thorpe and Emanuel's (1985) model.

Some information in the detailed structure of the fields of horizontal divergence and vertical motion was derived from the MIT Doppler radar data, through use of a volume-velocity processing technique (Waldteufel and Corbin, 1979). Results were provided by Dr. Neil D. Gordon (personal communication, 1985). This method produces results similar to those obtained from the VAD technique (Browning and Wexler, 1968), but uses all the data within the cylindrical volume rather

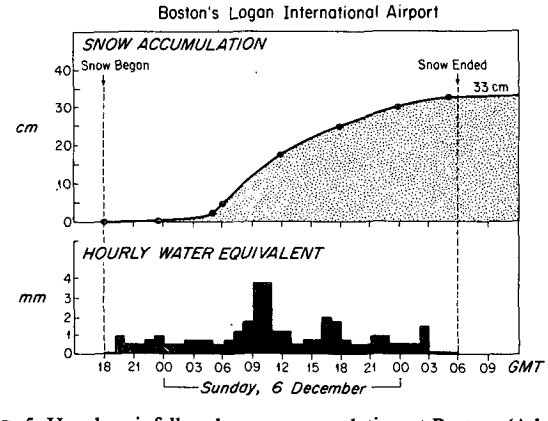

FIG. 5. Hourly rainfall and snow accumulation at Boston. (Adapted from U.S. Dept. of Commerce 1981.)

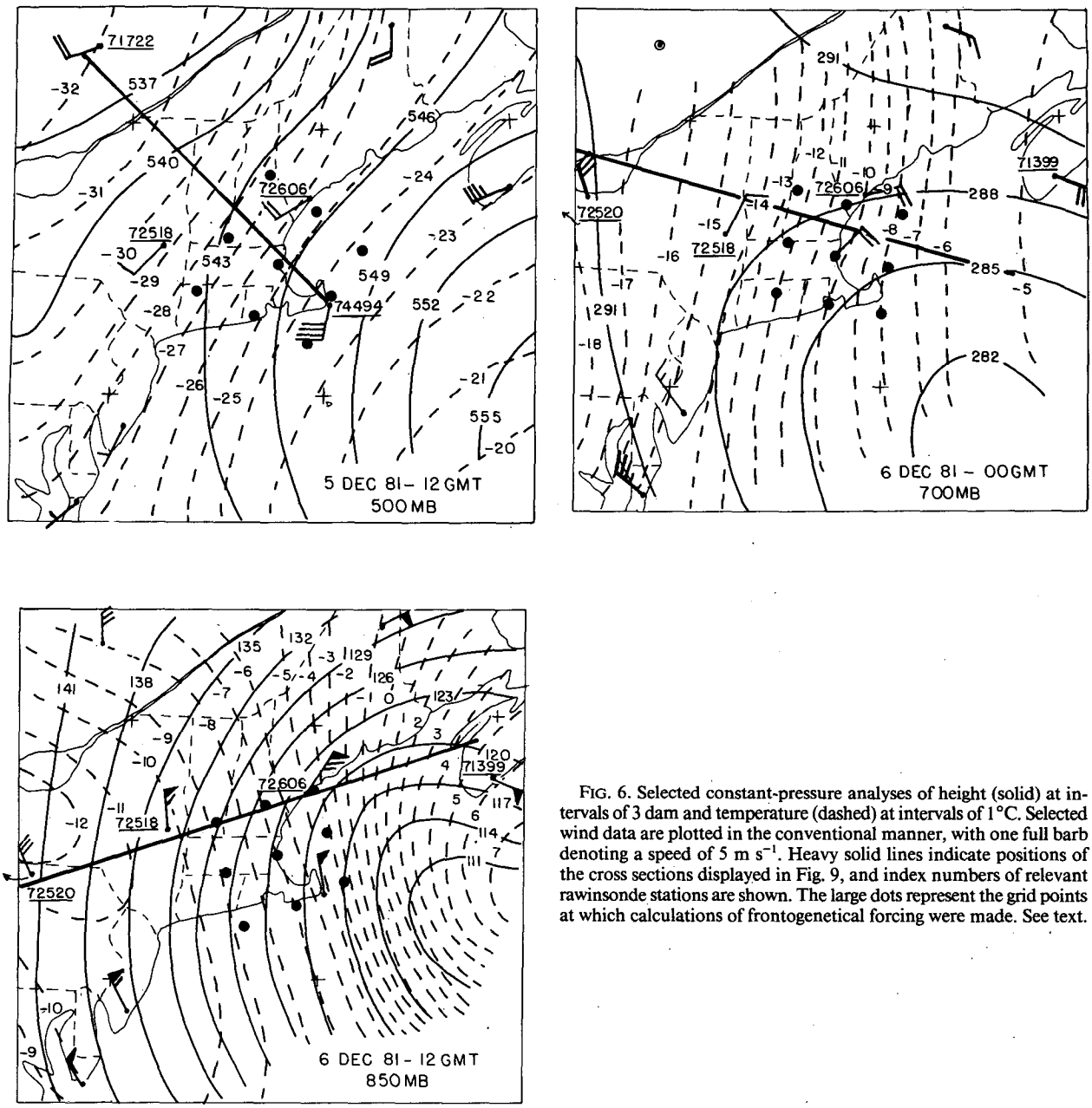

FIG. 6. Selected constant-pressure analyses of height (solid) at intervals of 3 dam and temperature (dashed) at intervals of 1 °C. Selected wind data are plotted in the conventional manner, with one full barb denoting a speed of 5 m s^{-1}. Heavy solid lines indicate positions of the cross sections displayed in Fig. 9, and index numbers of relevant rawinsonde stations are shown. The large dots represent the grid points at which calculations of frontogenetical forcing were made. See text.

than only data on its surface. Time sections of means for a cylindrical volume of radius 30 km appear in Fig. 8, for the period from 1400 GMT on the 5th, when sufficient targets were first available, until 0500 GMT on the 6th, when the taking of data for this purpose terminated. The wind velocity field (Fig. 8a) shows veering with height and a backing with time. Two speed maxima are apparent—one in south-southeasterlies at the highest level observed, around the time of the beginning of snowfall, and the other in northerly flow near 1 km elevation as the strengthening storm approached, toward the end of the period of observation. The level of maximum forcing (from Fig. 7) lay initially in south-southeasterly flow and finally in north-northeasterlies. Resemblance to the structure shown by Sanders and Bosart (1985b) for another major New England snowstorm is striking.

The most prominent feature of the divergence field (Fig. 8b) is a band of strong convergence, descending from 6 km elevation to 3 km during the period of observation. Simultaneously, the elevation of maximum frontogenetical forcing descended, remaining 0.5–1.0 km below the strongest convergence. This structure, viewed as a spatial variation, is in good agreement with

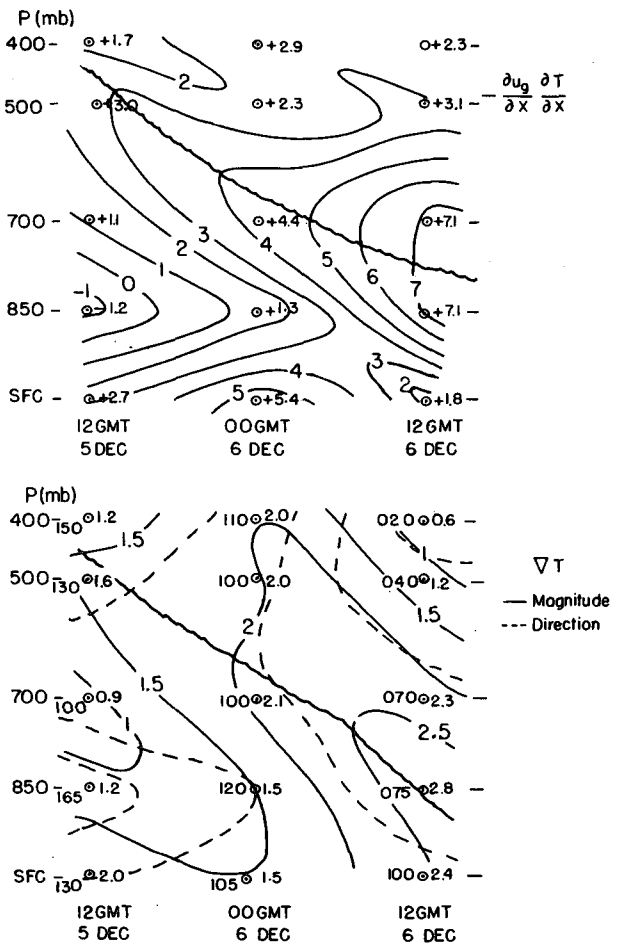

FIG. 7. Vertical time sections over New England of large-scale frontogenetical forcing (upper portion) in units of 1.04×10^{-10} °C m^{-1} s^{-1} and of horizontal temperature gradient (lower portion) with direction in deg (dashed) and magnitude in units of 0.9×10^{-5} °C m^{-1} (solid). Heavy wavy line indicates locus of maximum frontogenesis in upper portion and of maximum horizontal gradient in lower portion.

that calculated by Thorpe and Emanuel (1985) for the case of small symmetric stability in the ascending saturated air.

The field of vertical motion, shown in Fig. 8b, was calculated by upward integration of the equation of continuity, with $w = 0$ at the lower limit of the data as the boundary condition. (Before the echoes reached the ground, weak descent was probably occurring at this lower limit, so that the computed ascent aloft may have been excessive at this time.) Strong ascent was found only above 2.5 km elevation, as in the entire duration of the storm described by Sanders and Bosart (1985b). This pattern is also consistent with Thorpe and Emanuel's (1985) results, but in this case it is not possible to say with assurance how near the ground strong convergence and ascent descended, in the vicinity of MIT during the storm.

Details of the structure displayed in Fig. 8, however, cannot be explained by large-scale frontogenetical forcing. Note in particular the layering of additional lines of convergence and divergence across the zone of maximum forcing, with a vertical wavelength of 2–3 km, and also the splitting and reorganization of the main convergence band just before 0000 GMT. The reorganized band corresponded to the radar echo line illustrated in Fig. 4, while the earlier convergence was only weakly and intermittently suggested by the radar imagery (e.g., Fig. 3, 1157 GMT on the 5th). Cellular structure within the radar bands and within the vertical motion pattern was noticeable. Comparable features were seen in the snowstorm studied by Sanders and Bosart (1985b) and were attributed to symmetric instability.

4. Symmetric instability

a. Geostrophic diagnosis

To enable an assessment of the role of this instability, we prepared a set of vertical cross sections along lines parallel to the direction of the tropospheric-mean temperature gradient, optimally located with respect to the available rawinsondes and passing as closely as possible to MIT. The lines appear in Fig. 6. The x-axis lies along each line, directed toward the warmer air. The locations of the sounding stations were projected normally on the section lines.

The analysis began with a careful mapping of the field of potential temperature, θ, in the plane of the section. The field of geostrophic wind component normal to the section, v_g, was next constructed at each rawinsonde station by upward integration of the thermal-wind equation,

$$\frac{\partial v_g}{\partial p} = -\frac{R}{fp}\left(\frac{p}{1000}\right)^{0.285}\frac{\partial \theta}{\partial x}$$

with increments of 50 mb in pressure and 100 km in the x-distance. Independent measurements of v_g were made from analyses at the standard pressure levels, and the minor differences were reconciled by adjustment.

For a geostrophically balanced basic flow, the relevant momentum is given (e.g., Emanuel, 1983a) by $M_g = v_g + fx$. The fields of M_g were obtained by adding an appropriate value of fx to the analyzed v_g field, taking $x = 0$ at the left edge of each cross section and f as the value of the Coriolis parameter at the mean latitude. For an unsaturated atmosphere in geostrophic balance, symmetric instability is present if the θ surfaces are more steeply sloped than the M_g surfaces. For a saturated atmosphere an appropriately conservative thermodynamic property is the wet-bulb potential temperature, θ_w, and the comparison is between the slopes of surfaces of M_g and θ_w. Accordingly, the θ_w field was

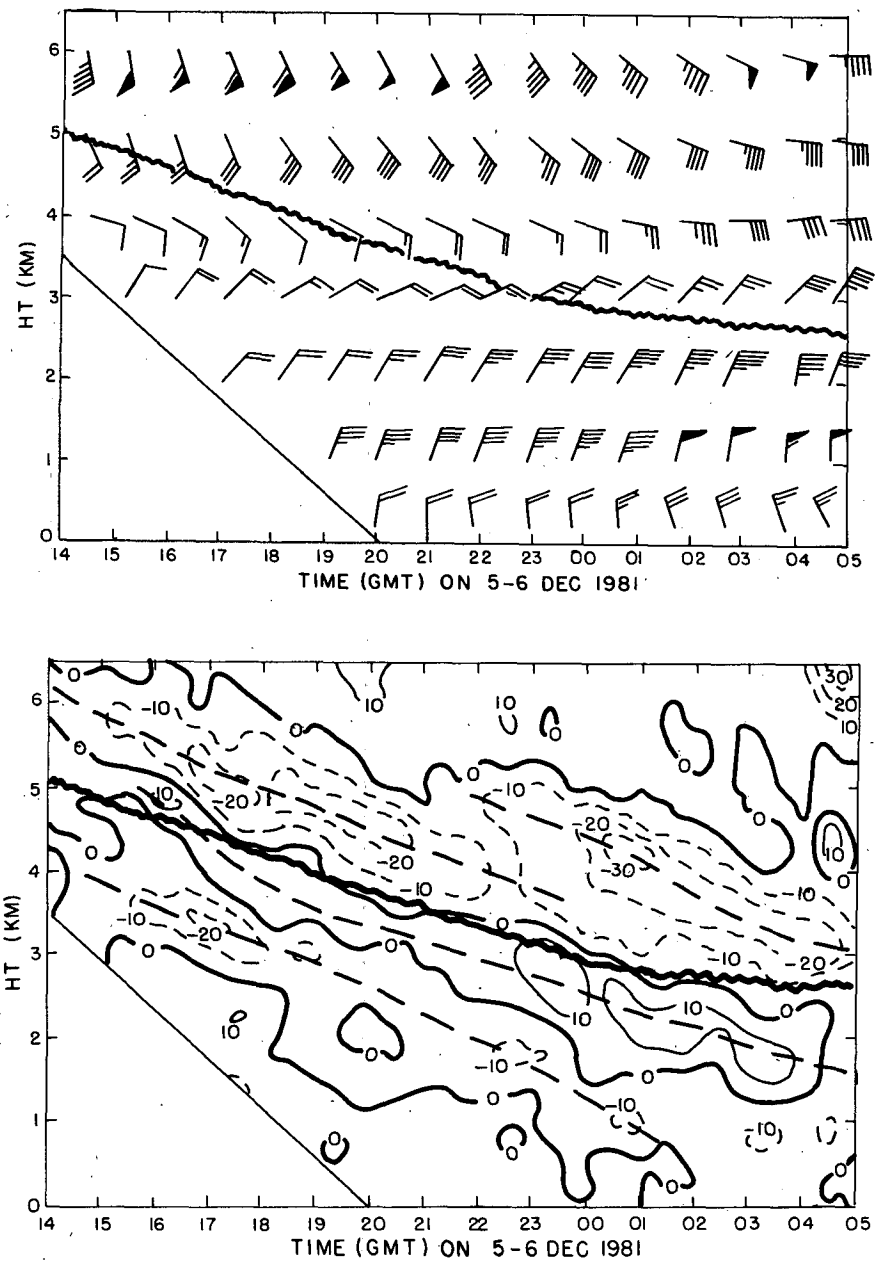

FIG. 8. Vertical time sections of (a) horizontal wind velocity, (b) divergence and (c) vertical motion, all derived from MIT Doppler radar. See text. Wind is plotted in conventional notation with vertical orientation representing north and one full barb representing 5 m s^{-1}. Divergence is in units of 10 s and heavy dashed lines represent lines of maximum divergence or convergence. Vertical motion is in cm s^{-1}. Heavy wavy line is locus of maximum frontogenetical forcing, from Fig. 7.

obtained from the soundings and was analyzed by assuring consistency with the θ field.

Cross sections of M_g and θ_w along the lines shown in Fig. 6 appear in Fig. 9. The hatched areas of nominal saturation were estimated from a dewpoint depression of 4°C or less in the soundings or from cloudiness evident in the infrared satellite imagery. The dashed outlines of the areas of symmetric instability for geostrophic flow were determined by comparison of the slopes of θ_w isotherms in the saturated areas or of θ isotherms (not shown) in the unsaturated areas, with the slopes of the M_g isopleths.

The unstable areas so determined were not extensive and were of two types—regions of upward decrease of θ_w in the nearly saturated boundary layer and deeper layers entirely (except at 1200 GMT on the 5th) within

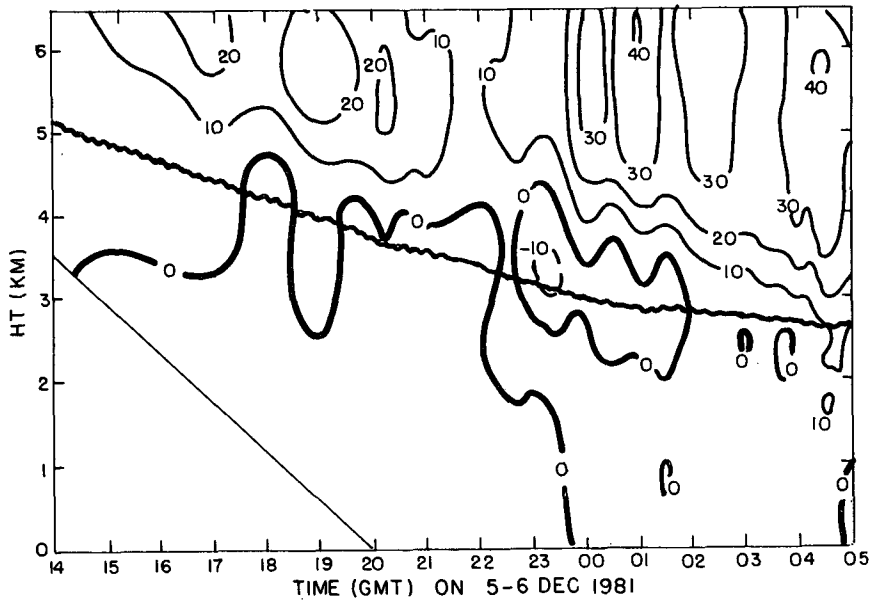

FIG. 8. (*Continued*)

the major cloud mass associated with the storm. The former regions were likely susceptible to shallow ordinary convection and perhaps to Ekman-layer instabilities, and the inviscid geostrophic theory does not seem germane. The latter regions were characterized by only modest vertical geostrophic shear but by relatively shallow M_g isopleths (attributable to strong anticyclonic lateral shear) and by relatively steep θ_w isotherms (reflecting small hydrostatic stability). These regions, however, extended downward no farther than about the 575-mb level and westward insufficiently far to encompass outlying bands seen in the satellite imagery beyond the main cloud mass.

These results can be compared with those obtained by Passarelli et al. (1986) at 74494 (Chatham) at 1200 GMT on the 5th and at 72606 (Portland) 12 h later by calculation of a Richardson number from data for an individual sounding. It was assumed that the observed vertical wind shear was in geostrophic balance and that there was no lateral shear in v_g.

At 74494 an unstable region was found from 4.4 to 6.0 km (their Fig. 6), whereas our analysis (Fig. 9a) shows instability from 5.3 to 6.4 km (510–440 mb). This degree of agreement seems fortuitous, since 1) the Richardson number calculation was based on dry thermodynamics, which would have yielded stability throughout according to our analysis; 2) our geostrophic analysis is precarious at this station, owing to lack of sounding data to the southeast; and 3) the vertical shear in this region may have been substantially supergeostrophic, as will be seen.

At 72606, at 0000 GMT on the 6th, the Richardson number analysis (Passarelli et al., 1986, Fig. 11) yielded a shallow unstable layer just below 3 km elevation, evidently to be identified with the upper portion of the small unstable region in our Fig. 9b near the 700-mb level. The lower portion of our region reflected a shallow layer of upward decrease in θ_w, evidently not resolved by the calculation of Passarelli et al. (1986), but not a realistic indication of symmetric instability, either. A more important discrepancy is the failure of the single-station method to show any instability in the middle troposphere. This is seen in Fig. 9b to occur in a region of small lateral variation of M_g, i.e., of anticyclonic shear, which, of course, cannot be detected in a single sounding.

By 1200 GMT on the 6th, the only unstable regions (Fig. 9c) were those where θ_w decreased upward. No significant symmetric instability was indicated.

b. Gradient wind effects

It was noted during analysis that winds tended to be markedly supergeostrophic in the middle to upper troposphere over New England during the early part of the storm. As an illustration, Fig. 10 displays the ageostrophic component normal to the plane of the cross section for 1200 GMT on the 5th. The flow at and above the 500-mb level at this time was south-southwesterly, nearly normal to the plane, so that a positive value of $v - v_g$ denotes a supergeostrophic condition. Note at both 72518 and 72606 the marked upward increase of this ageostrophic component in the layer from 500 mb to a peak between 350 and 300 mb (the level of the tropopause) and then a rapid decrease. There is a suggestion of similar behavior at 74494, with

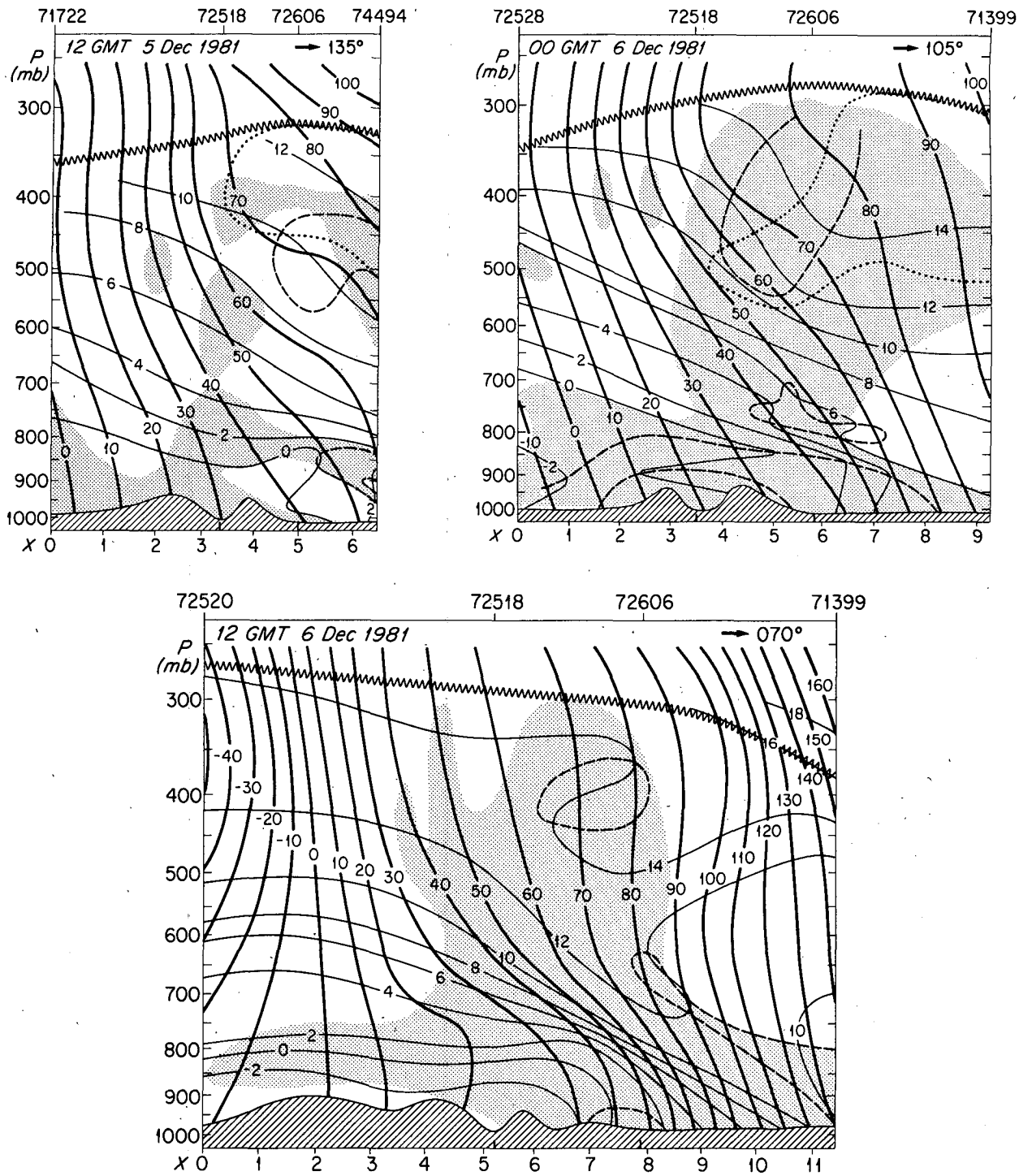

FIG. 9. Vertical cross section of θ_w (thin solid) and of M_g (heavy solid) along lines shown in Fig. 6. Dashed lines enclose areas of symmetric instability derived from the geostrophic analyses, while dotted lines similarly denote areas derived from the gradient-wind analyses. Heavy wavy line denotes the tropopause. Stippling indicates regions of nominal saturation. Projected positions of sounding stations are shown by index number along top of diagram. At bottom of diagram, land profile is shown by hatching, and distance in the x-direction (toward warmer air) is indicated in hundreds of kilometers. Geographic orientation of the x-axis is shown in upper-right portion of diagram.

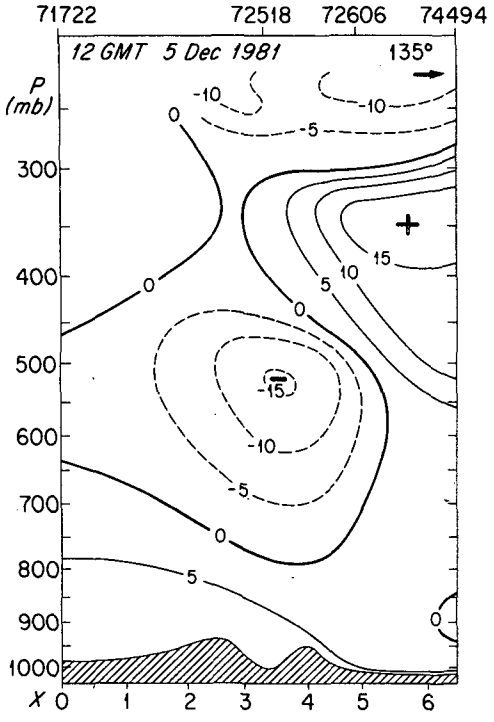

FIG. 10. Vertical cross section as in Fig. 9a, except for $v - v_g$. Isotachs at intervals of 5 m s^{-1}.

supergeostrophic vertical shear (cf. discussion in the preceding section) in the layer from 590 to 460 mb (4.2–6.1 km). Here the observed component, v, increased by 23 m s^{-1} while the analyzed geostrophic counterpart increased only 14 m s^{-1}. Of course, the analysis is uncertain in the vicinity of this station, as pointed out above, but comparable discrepancies at the other two stations occurred where the geostrophic analysis is relatively certain.

It is recognized (Eliassen, 1952; Schubert and Hack, 1983; Thorpe, 1985) that vanishing absolute vorticity is a condition for symmetric neutrality for a circular vortex in gradient wind balance. The geostrophic analysis can be extended and modified by assuming as an approximation that the atmosphere can be modeled locally as a portion of such a vortex. We do not pretend to justify this assumption a priori, but rather regard the application of this analysis as heuristic. For a ring of parcels displaced along an appropriate thermodynamic surface in such a vortex with constant f, the absolute angular momentum of the tangential motion,

$$vr + fr^2/2$$

about the center at $r = 0$ is conserved. From this it follows that

$$dv/dr = -v/r - f,$$

where d/dr refers to the change following a parcel along the relevant thermodynamic surface. During this displacement, the changes experienced by the parcels in the horizontal pressure-gradient force, the Coriolis force and the centrifugal force are, respectively, $-fd\bar{v}_g/dr$, $-(fv/r + f^2)$ and $-3(v/r)^2 - 2fv/r$, where the overbar refers to the basic state. For neutral stability, the velocity of the parcels in the ring must remain the same as the velocity in the environment experienced by them. If this environment is in gradient-wind balance, then $v = \bar{v}_{gr}$ and the sum of the changes in the three forces must equal zero.

This consideration gives as the criterion for symmetric neutrality,

$$\frac{d\bar{v}_g}{dr} = \frac{-3\bar{v}_{gr}}{r}\left(1 + \frac{\bar{v}_{gr}}{fr}\right) - f. \tag{1}$$

Identifying dr with dx in the context of our analysis, we can write (1) as

$$\frac{d\bar{v}_g}{dr} + f = \frac{d\bar{M}_g}{dx} = \frac{-3\bar{v}_{gr}}{r}\left(1 + \frac{v_{gr}}{fr}\right). \tag{2}$$

When r approaches infinity, we have in the limit from (2) that $\bar{M}_g$ does not vary along the path of the displaced parcel, the condition for neutrality in geostrophic flow. If the rate of change of $\bar{v}_g$ or $\bar{M}_g$ with r (or x) is algebraically less than the value given by (1) or (2), then the flow is symmetrically unstable.

The criterion (1) can be shown to represent vanishing absolute vorticity for a vortex in gradient balance, a general condition for symmetric neutrality, as mentioned earlier. Equations (1) and (2) express this neutrality in relatively complex terms. They are more convenient than they may appear, however, since thermal wind analysis in a form such as we have used seems almost indispensable, and the geostrophic criteria are standard ones from which deviations can be taken to account for gradient-wind effects. (As pointed out by Thorpe, 1985, the counterpart of M_g for a circular gradient wind is $R = r(1 + 2v_{gr}/fr)^{1/2}$. In real flow patterns, however, the resemblance to such a vortex is local at best, so that use of R appears to be impractical).

A device for aiding determination of these deviations is presented in Fig. 11. These nomograms give the rates of change of v_g or M_g with distance (along the x-axis in our case) for gradient symmetric neutrality, as a function of the geostrophic speed and the radius of curvature of the trajectory. (Here and subsequently we dispense with the overbar.) They are applicable most readily when the flow is parallel to the thermal wind. In Fig. 11, which refers to conditions at latitude 40 deg, we see that with appreciable geostrophic speed and cyclonically curved trajectories, extraordinary anticyclonic *geostrophic* shear is required for instability. Put another way, negative absolute vorticity is not likely to be found in pronounced troughs in the middle and upper troposphere. With anticyclonically curved trajectories, on the other hand, relatively modest *geostrophic* shears are required. In the limiting anticyclonic

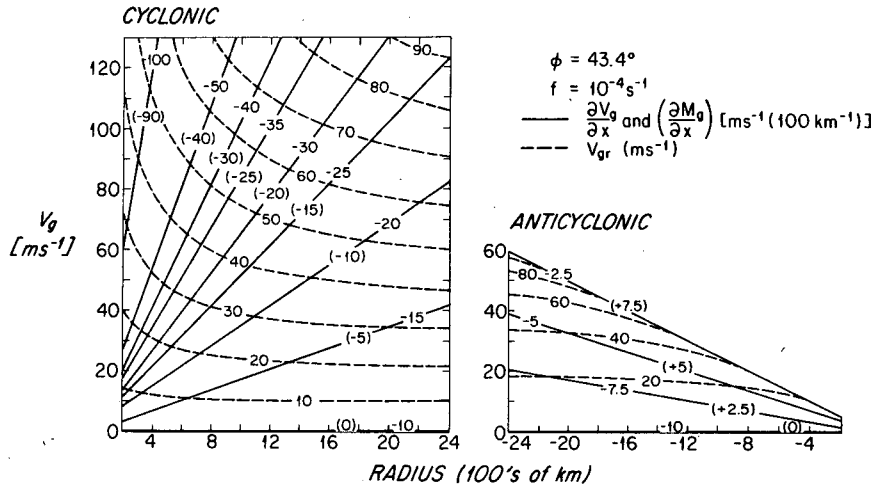

FIG. 11. Nomograms for determining (solid lines) critical values of shear of v_g and of M_g for symmetric neutrality and (dashed lines) values of gradient wind speed, given the values of geostrophic speed, V_g, and radius of trajectory curvature, r. On solid lines the values refer to $\partial v_g/\partial x$, while additional values in parentheses refer to $\partial M_g/\partial x$. The nomograms are for 43.4 deg latitude.

case where the gradient-wind speed is twice the geostrophic value, the critical geostrophic shear is only $-f/4$, while the critical value of $\partial M_g/\partial x$ is $3f/4$. It appears that negative absolute vorticity is relatively likely to be found in upper ridges.

We do not mean to suggest that a mechanism for production or suppression of negative vorticity resides necessarily in upper troughs and ridges. To the contrary, the potential vorticity (Ertel, 1942) is a highly conservative property, and the mechanisms of its generation or destruction are beyond the scope of this study. We suggest only that since this vorticity tends to be conserved, and since the upper-level winds tend to blow through the troughs and ridges, these features represent the equatorward and poleward limits, respectively, of a given trajectory. One might argue, then, that the potential vorticity deviations should be positive and negative at the trough and ridge, respectively, owing simply to the meridional variation of f.

The dependence of the data in Fig. 11 upon latitude is displayed in Table 1 for a reasonably robust pair of values of v_g and r. Note that δv_g and δM_g, the critical changes in a distance of 100 km, vary only modestly over the range of latitudes where analysis is likely to be undertaken. The latter change is nearly constant from the pole to latitude 40 deg, since the variation in δv_g is nearly balanced by the variation of f. The sensitivity to latitude increases with decreasing radius of curvature, as suggested by Eq. (2).

For application to a particular case, it is necessary to estimate the radius of trajectory curvature. Except where the wind is strongly influenced by a high-frequency disturbance, a representative value of r can be obtained by noting that the equation of inviscid motion in the direction normal to the observed wind can be written

$$f(V-V_{gs})=-V^2/r, \quad \text{or} \quad r=-V^2/[f(V-V_{gs})],$$

where V is the observed wind speed and V_{gs} is the component of geostrophic wind in the direction of the observed wind. The radius of curvature could be obtained, in principle, from a series of nomograms such as those shown in Fig. 11, since at a given latitude a pair of values of V_g and V (assumed to be equal to V_{gr}) determines r. Such a pair further determines $\delta M_g/\delta x$ on the assumption that V is normal to the plane of the section and hence to the temperature gradient and parallel to

TABLE 1. Critical values of $\partial v/\partial x$, $\partial M_g/\partial x$ (m s^{-1}/100 km) for symmetric neutrality, in gradient flow, as a function of latitude, ϕ, for v_{gr} = 41 m s^{-1}, r = 1481 km. Values in parentheses refer to the case of geostrophic balance ($r = \infty$).

ϕ (deg)	v_g	$\partial v_g/\partial x$	$\partial M_g/\partial x$	Geostrophic
		Cyclonic		
90	49	−24	−10	(−14)
80	49	−24	−10	(−14)
70	49	−24	−10	(−14)
60	51	−23	−10	(−13)
50	52	−21	−10	(−11)
40	54	−20	−11	(−9)
30	57	−19	−12	(−7)
20	64	−18	−13	(−5)
		Anticyclonic		
90	34	−7	7	
80	34	−7	7	
70	33	−7	7	
60	32	−6	7	
50	31	−5	6	
40	29	−4	6	
30	26	−2	5	
20	Gradient balance not possible			

TABLE 2. Estimates of trajectory curvature, r (km) and of $\partial M_g/\partial x$ (m s^{-1} 100 km) for symmetric neutrality over central New England, December 1981. Coriolis parameter, $f = 9.81 \times 10^{-5}$ s^{-1}. Speeds in m s^{-1}. Angles and directions in deg.

Date	Time (GMT)	Level (mb)	Station pair	V	α	V_{gr}	r	$\partial M_g/\partial x$
5	1200	850	72518, 74494	014/09.1	98	8.2	−938	+2.6
5	1200	700		Winds light and variable				—
5	1200	500	72518, 74494	193/12.4	81	17.1	+333	−15.4
5	1200	400	72518, 74494	197/32.7	85	22.6	−1079	+6.3
5	1200	300	72518, 74494	212/34.5	100	34.3	−60665	+0.0
6	0000	850	72518, 72606	023/15.2	49	15.0	−11776	+0.0
6	0000	700		Winds parallel to line between stations*				>0
6	0000	500	72518, 72606	153/15.2	81	13.1	−1121	+3.5
6	0000	400	72518, 72606	157/25.2	85	29.1	+1660	−5.2
6	0000	300	72518, 72606	155/36.3	83	39.0	+4975	−2.4
6	1200	850	72518, 72606	014/29.5	58	43.7	+624	−21.0
6	1200	700	72606, 74494	066/15.7	105	21.4	+441	−14.6
6	1200	500	72606, 74494	057/14.9	114	29.5	+155	−57.1
6	1200	400	72518, 72606	069/23.1	**	27.3	+1295	−6.3
6	1200	300	72518, 72606	077/27.6	**	26.8	−9706	+0.8

* 74494 sounding missing.

** 74494 sounding terminated below 400 mb. Wind nearly parallel to line joining alternative station pair. Geostrophic wind estimated from analysis.

V_{gr}. Application of the above formula, however, is more accurate and less restrictive.

For the series of maps of which Fig. 6 presents a sample, r was thus estimated for the area under surveillance of the MIT radar. To avoid the uncertainties of analysis and to purchase objectivity at the cost of acceptance of small errors in the data, estimates were made only at times and levels (above the surface) where the line connecting two soundings was oriented reasonably near normal to the wind. The speed of the vector-mean wind at the two stations was compared to an estimate of V_g obtained by dividing the geostrophic component determined by the difference in pressure-heights at the two stations by $\sin\alpha$, α being the difference between the direction of the line connecting the two stations and the direction of the vector-mean observed wind. Results appear in Table 2.

Comparing the data in Table 2 with the geostrophic analyses in Fig. 9a, we find from the variation of M_g along θ_w surfaces that the entire upper troposphere between 72518 and 74494 becomes symmetrically unstable, whereas the extension to and below 500 mb is eliminated by the gradient-wind model. The analysis at and southeast of 74494 is uncertain owing to the lack of sounding data. The detached area of saturation near 500 mb between 71722 and 72518, reflecting a prominent streak of cloud in the satellite imagery (not shown), lay in a region of strong symmetric stability irrespective of gradient wind effects. It was propagating to the left of the flow at 10–15 m s^{-1} at this time, suggestive of the character of a gravity wave.

Gradient wind effects at 0000 GMT on the 6th (Table 2 and Fig. 9b) show over New England a modest enhancement of instability near 500 mb but elimination of it above this level. Moreover, calculations similar to those in Table 2, but for the segment between 72606 and 71399, indicated a large region of decidedly supergeostrophic wind and instability in the middle and upper troposphere here.

It appears that the 72606 rawinsonde-reported temperatures and heights may have been somewhat too high at and above 500 mb. If so, the winds would be apparently subgeostrophic to the left and supergeostrophic to the right of this station, despite anticyclonic curvature of streamlines over the entire region in a massive ridge preceding the storm. To obtain information independent of the questionable height data at 72606, weighted average results were obtained for the entire segment from 72518 to 71399. For 500, 400 and 300 mb, respectively, we found averaged anticyclonic radii of curvature of 1309, 1803 and 2013 km, and averaged critical values of $\partial M_g/\partial x$, in m s^{-1}/100 km, of +3.6, +3.7 and +4.1. It is seen from Fig. 9b that much of the major cloud mass at and above 500

TABLE 3. Change of M_g, δM_g, from 72518 to 72606 (m s^{-1}/100 km) along selected surfaces of wet-bulb potential temperature, θ_w, (°C) 6 December 1981.

θ_w	δM_g 0000 GMT	δM_g 1200 GMT
14	2.0	7.5
12	0.0	7.0
10	2.7	7.8
8	5.3	9.0
6	4.0	9.3
4	3.8	9.3
2	5.0	9.0

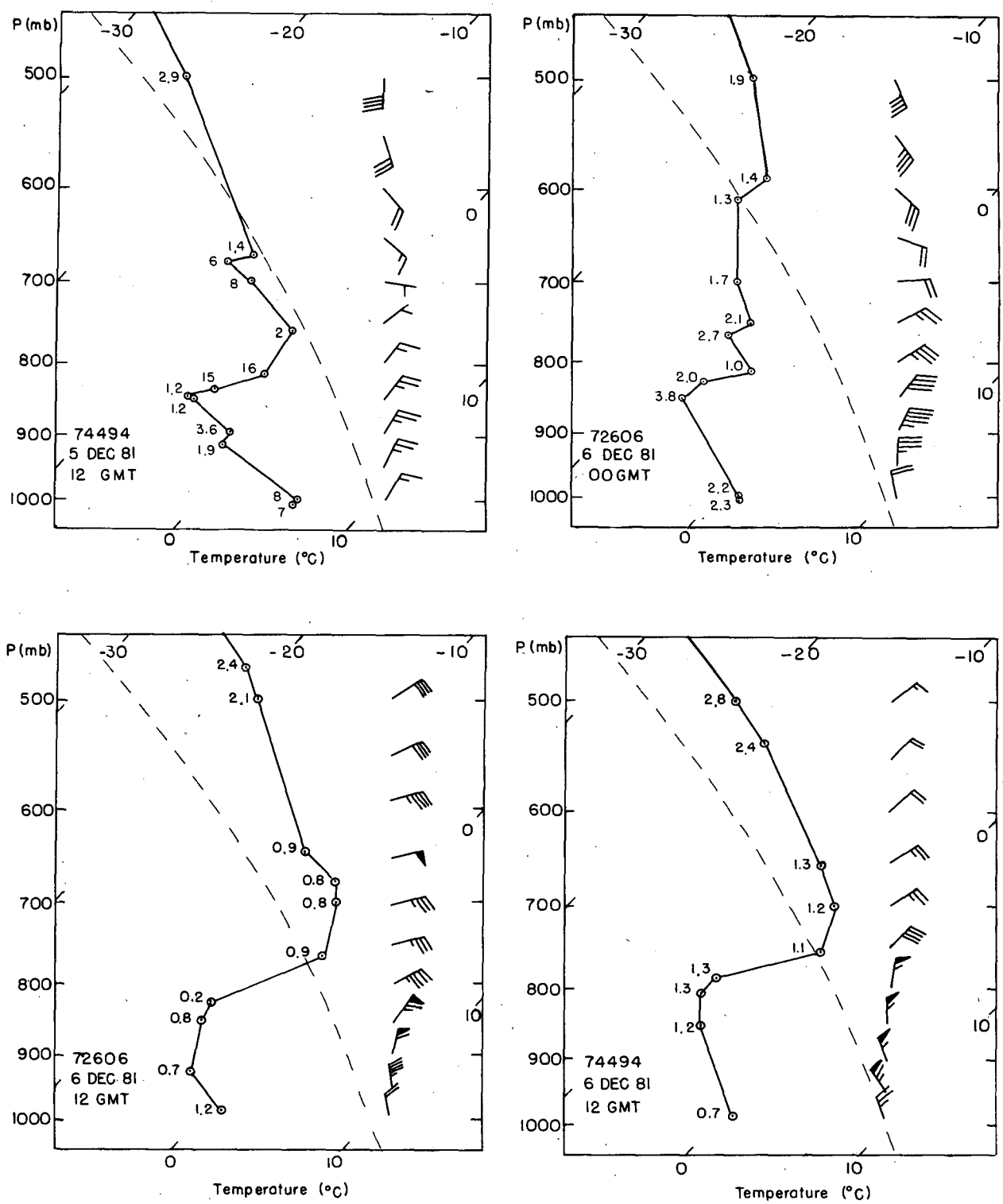

FIG. 12. Skew T–log p diagrams for selected soundings. Solid lines denote temperature profile. Dewpoint depression (°C) is given numerically to left of temperature points. Dashed line is saturation adiabat for θ_w = 10°C. Winds are plotted in conventional fashion with north understood to be upward, and with a full barb representing 5 m s^{-1}.

mb then would likely have been symmetrically neutral or unstable.

The small detached areas of saturation in the segment between 72518 and 72528 in Fig. 9b (derived from satellite imagery as in Fig. 9a) again lay in a very stable region.

By 1200 GMT on the 6th, the region had become much more stable on the basis of geostrophic analysis, as mentioned before. The change in the segment of Fig. 9c more or less within MIT radar surveillance is shown in Table 3. Note that at this later time, since f can be expressed as approximately 9.8 m s^{-1}/100 km, one would be hard put to find symmetric instability even with the limiting case of anticyclonic gradient flow, recalling that when $V_{gr} = 2V_g$, the critical value of $\partial M_g/\partial x$ is $3f/4$. This possibility aside, in Table 2 we see evidence of prominent cyclonic gradient flow, except near the tropopause at 300 mb, as the storm approached and extended its influence throughout the troposphere. The cloud striations west of 72518 remained near the outer edge of the storm circulation. Satellite imagery showed the individual bands to be transient phenomena, each propagating westward or northwestward for several hours before dissipating.

5. A note on frontal structure

Since strong geostrophic frontogenetical forcing was occurring over New England during the 24-h period under study, it is interesting to examine the relevant soundings for evidence of frontal structure. At 1200 GMT on the 5th and 0000 GMT on the 6th such evidence was slim. Examples are shown in Figs. 12a and 12b. No prominent inversion or stable layer accompanied the strong vertical wind shear signifying the frontal zone, although the upward decrease of dewpoint depression from the dry air below to the saturated air above was often dramatic. Evidently the difference between the adiabatic warming in the cold air below and the cooling in the warm air above was sufficient to nullify much of the development of a stable layer produced by the ageostrophic horizontal part of the frontal circulation as well as the growth of horizontal temperature gradient (as seen in Fig. 7) produced by geostrophic confluence. The contrast in humidity, on the other hand, is enhanced by the frontogenetical circulation, a result illustrated by Fig. 12a. By 0000 GMT on the 6th, however, after substantial precipitation had fallen, the colder air had evidently been moistened by evaporation. This situation is exemplified by conditions at 72606 (Fig. 12b) if we assume that no strong ascent here occurred below 3–4 km, as in the vicinity of MIT (cf. Fig. 8c).

At 1200 GMT on the 6th, when the frontal zone had descended toward the lower troposphere, it was characterized by a marked inversion layer at 72606 and 74494, as seen in Figs. 12c and 12d. Evidently the adiabatic effects here were unable to undo effectively the effects on the temperature field produced by the horizontal limbs of the frontal circulation. The values of θ_w at the top of this layer approximated those at the surface in the easterly flow north of the cyclone center, as seen in Fig. 13. In the detailed depiction of plotted data, the front extending northwestward from the low center seems quite pronounced in the contrast of temperature and wind between the ship PEWI and the buoys 44005 and 44003. It did not appear in the NMC analysis (Fig. 1c) but would match nicely the frontal inversions in Figs. 12c and 12d, with a slope of about 1:100. This front was evidently responsible for the banded precipitation structure seen in the radar patterns over southeastern New England at about this time (Fig. 3 at 0803 GMT and 1224 GMT on the 6th), despite probably large potential vorticity and symmetric stability.

The vertical wind shear in these last two soundings was so large that the Richardson number,

$$\mathrm{Ri} = \frac{\eta}{f}\frac{\Gamma_m}{\Gamma_d}\frac{g}{\theta_e}\frac{\partial\theta_e/\partial z}{(\partial V/\partial z)^2}$$

discussed by Sanders and Bosart (1985a) and used by Seltzer et al. (1985) and by Passarelli et al. (1986), was close to the critical value of 1. With the ratio of absolute vorticity to coriolis parameter, η/f, taken equal to 1 and the observed wind used to evaluate the vertical shear, values of 1.4 and 0.8, respectively, were found

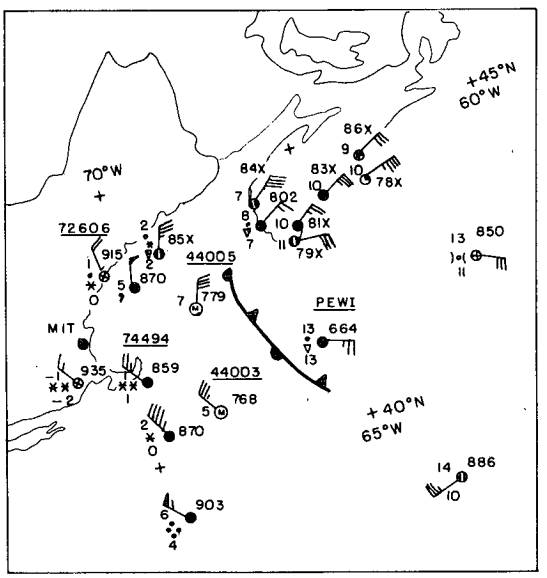

FIG. 13. Surface data, plotted in conventional manner, for 1200 GMT 6 December. Identity of selected observations indicated by underlined index number or radio call sign.

for the layer from 810 to 700 mb at 74494 and for the layer from 890 to 765 mb at 72606. Strong cyclonic horizontal shear at the latter station, as indicated by the cross-section analysis in Fig. 9c, suggests a value of about 2.5 for η/f in the frontal layer here, eliminating the suggested instability. The danger of relying on single-station evaluation of the Richardson number in an active synoptic situation is evident.

6. Concluding summary

We have examined the synoptic and radar information for the major New England snowstorm of 5–6 December 1981, which occurred as an explosively deepening cyclone moved northward offshore. The synoptic-scale patterns of pressure and temperature showed frontogenetical forcing over a broad area ahead and to the left of the track of the storm. Symmetric stability was small in the warmer air in the middle and upper troposphere at the leading portion of the storm. In fact, if some crude account is taken of the effect of centrifugal force by assuming that the atmosphere locally resembled a steady circular vortex in gradient wind balance, symmetric instability was present in this region.

A major band of ascent aloft was closely related to the forcing, so that frontogenesis is regarded as the driving mechanism. The role of the small symmetric stability was to enhance the intensity of the frontal circulation and, where it was negative, to produce structural details. The most persistent and prominent of these was a long band at the leading (northwestern) edge of the precipitation area. Most of the snow fell not with this band but later as increasingly stable air with larger potential vorticity filled the inner portion of the cyclone, producing a more chaotic radar appearance.

This diversity and evolution distinguished this storm from the Megalopolitan Snowstorm of 11–12 February 1983, studied in detail by Sanders and Bosart (1985a,b), in which a single major band dominated nearly throughout and produced nearly all the snow. The two storms were similar, however, in that the main ascent occurred well above the surface. This ageostrophic circulation in both cases was driven by large-scale frontogenetical forcing with small symmetric stability acting both as catalyst and as provider of structural detail.

Acknowledgments. The author benefited from discussions with Kerry Emanuel, MIT, Rich Passarelli, SIGMET, Inc., and Neil Gordon, New Zealand Meteorological Service. He is grateful to the Center for Meteorology and Physical Oceanography, MIT, for access to data and provision of facilities, and to Isabelle Kole and Mike Rocha for preparation of illustrations. This work was supported by the National Science Foundation under Grant ATM-8407142.

REFERENCES

Bennetts, D. A., and B. J. Hoskins, 1979: Conditional symmetric instability—a possible explanation for frontal rainbands. *Quart. J. Roy. Meteor. Soc.*, **105,** 945–962.

Bjerknes, J., 1919: On the structure of moving cyclones. *Geofys. Publ. Norske Videnskaps-Akad.*, **1,** 1–8.

Browning, K. A., and R. Wexler, 1968: A determination of kinematic properties of a wind field using Doppler radar. *J. Appl. Meteor.*, **7,** 105–113.

——, and T. W. Harrold, 1969: Air motion and precipitation growth in a wave depression. *Quart. J. Roy. Meteor. Soc.*, **95,** 288–309.

Eliassen, A., 1952: Slow thermally or frictionally controlled meridional circulation in a circular vortex. *Astrophys. Norv.*, **5,** 60 pp.

Elliott, R. D., and E. L. Hovind, 1964: On convection bands within Pacific Coast storms and their relation to storm structure. *J. Appl. Meteor.*, **3,** 143–154.

Emanuel, K. A., 1983a: The Langrangian parcel dynamics of moist symmetric instability. *J. Atmos. Sci.*, **40,** 2368–2376.

——, 1983b: On assessing local conditional symmetric instability from atmospheric soundings. *Mon. Wea. Rev.*, **111,** 2016–2033.

——, 1985: Frontogenesis in the presence of low moist symmetric stability. *J. Atmos. Sci.*, **42,** 1062–1071.

Ertel, H., 1942: Ein neuer hydrodynamischer Wirbelsatz. *Meteor. Z.*, **59,** 271–281.

Herzegh, P. H., and P. V. Hobbs, 1980: The mesoscale and microscale structure and organization of clouds and precipitation in midlatitude cyclones. Part II: Warm frontal clouds. *J. Atmos. Sci.*, **37,** 597–611.

Hoskins, B. J., and M. A. Pedder, 1980: The diagnosis of middle latitude synoptic development. *Quart. J. Roy. Meteor. Soc.*, **106,** 707–720.

——, E. C. Neto and H. -R. Cho, 1984: The formation of multiple fronts. *Quart. J. Roy. Meteor. Soc.*, **110,** 881–896.

Hsie, E. -Y., R. A. Anthes and D. Keyser, 1984: Numerical simulation of frontogenesis in a moist atmosphere. *J. Atmos. Sci.*, **41,** 2581–2594.

Kreitzberg, C. W., 1968: The mesoscale wind field in an occlusion. *J. Appl. Meteor.*, **7,** 53–67.

Passarelli, R. E., Jr., and H. Boehme, 1983: The orographic modulation of pre-warm-front precipitation in southern New England. *Mon Wea. Rev.*, **111,** 1062–1070.

——, N. D. Gordon and M. A. Seltzer, 1986: Case study of an intense winter snow band: The possible role of symmetric instability. [Submitted to *J. Atmos. Sci.*]

Sanders, F., and L. F. Bosart, 1985a: Mesoscale structure in the megalopolitan snowstorm of 11–12 February 1983. Part I: Frontogenetical forcing and symmetric instability. *J. Atmos. Sci.*, **42,** 1050–1061.

——, and ——, 1985b: Mesoscale structure in the megalopolitan snowstorm of 11–12 February 1983. Part II: Doppler radar study of the New England snowband. *J. Atmos. Sci.*, **42,** 1398–1407.

Sawyer, J. S., 1952: A study of the rainfall of two synoptic situations. *Quart. J. Roy. Meteor. Soc.*, **78,** 231–246.

Schubert, W. H., and J. J. Hack, 1983: Transformed Eliassen balanced vortex model. *J. Atmos. Sci.*, **40,** 1571–1583.

Seltzer, M. A., R. E. Passarelli and K. A. Emanuel, 1985: The possible role of symmetric instability in the formation of precipitation bands. *J. Atmos. Sci.*, **42,** 2207–2219.

Sutcliffe, R. C., and A. G. Forsdyke, 1950: The theory and use of upper air thickness patterns in forecasting. *Quart. J. Roy. Meteor. Soc.*, **76,** 189–217.

Thorpe, A. J., 1985: Diagnosis of balanced vortex structure using potential vorticity. *J. Atmos. Sci.*, **42,** 397–406.

——, and K. A. Emanuel, 1985: Frontogenesis in the presence of small stability to slantwise convection. *J. Atmos. Sci.*, **42,** 1809–1824.

U.S. Dept. of Commerce, 1981: *Storm Data,* **23**(1), 43 pp.

Waldteufel, P., and H. Corbin, 1979: On the analysis of single Doppler radar data. *J. Appl. Meteor.*, **18,** 532–542.